Arch. Metall. Mater. **66** (2021), 2, 659-668

DOI: 10.24425/amm.2021.135904

B. HADAŁA[1], M. RYWOTYCKI[1*], Z. MALINOWSKI[1], SZ. KAJPUST[2], S. MISIOWIEC[2]

OPTIMIZATION OF LONG CHARGE HEATING IN A ROTARY FURNACE

Heat consumption and steel loss for scale determine the costs of a heating process. The heating rate influences both. This paper evaluates the heating rate of a long charge made of three various materials, depending on the changes of the furnace atmosphere on the rotary furnace circumference. Numerical computing was performed based on a formulated heat transfer model in the rotary furnace chamber, while considering the growth of the scale layer. One heating curve was selected, which has allowed the heating time to be reduced by 36% while limiting the scale loss by 40%. It was also shown that the thermal stresses and strains should not lead to fractures of the charge heated.

Keywords: long charge heating model, heating curve, rotary furnace

Nomenclature

A_{g2}	–	absorptivity of gas
B_w	–	charge width
c	–	specific heat
C_{RT}	–	constant
g_z	–	oxidized layer thickness, mm
k_i	–	coefficient
L	–	characteristic length
l	–	average thickness of the combustion gas layer
L_w	–	charge length
Nu	–	Nusselt number
P_g	–	transparency of the gas body
p_{H_2O}	–	partial pressure of water vapor
p_i	–	partial pressure of steam or carbon dioxide in flue gas
Pr	–	Prandtl number
q_{con}	–	convection heat flux
q_{rad}	–	radiation heat flux
$\dot{q}_v$	–	latent heat
Re	–	Reynolds number
t	–	charge temperature, °C
T_g	–	gas body temperature, K
T_1	–	furnace wall surface temperature, K
T_2	–	charge surface temperature, K
x_1, x_2, x_3	–	Cartesian coordinates
α_{gw}	–	convective heat transfer coefficient on the charge surface
α_w	–	effective heat transfer coefficient
α_2	–	equivalent heat transfer coefficient
σ_p	–	stress intensity
σ_m	–	average stress
ε_g	–	equivalent emissivity of flue gas
ε_{sw}	–	equivalent emissivity of walls-charge system
ε_w	–	emissivity of steel
ε_{CO_2}	–	emissivity of carbon dioxide
ε_{H_2O}	–	emissivity of water vapor
λ	–	thermal conductivity
λ_s	–	flue gas thermal conductivity coefficient
λ_z	–	scale thermal conductivity
ρ	–	density
ρ_z	–	scale density
τ	–	time
φ	–	view factor
$\overline{\varphi}_f$	–	effective logarithmic strain

1. Introduction

The heat consumption during the operation of heating furnaces can simultaneously be substantially reduced and their performance improved by applying a proper heating practice.

[1] AGH UNIVERSITY OF SCIENCE AND TECHNOLOGY, AL. A. MICKIEWICZA 30, 30-059 KRAKOW, POLAND
[2] ZARMEN FPA SP. Z O.O., 39 FILARSKIEGO STR., 47-330, ZDZIESZOWICE, POLAND
* Corresponding author: rywotyc@agh.edu.pl

The appropriate distribution of the thermal energy supplied to the charge in the furnace chamber is one of potential solutions. It involves designing a heating curve.

Rotary heating furnaces are used for heating the charge supplied to rolling mills. The furnaces usually operate in a counter-current system. The charge is delivered to the furnace through a charging door. Blooms are placed radially on the rotary hearth, and the hearth is shifted with a particular angle, at a particular time interval. The heated charge is discharged from the furnace through a discharge door. The furnace is divided into three zones: I preheating zone, II heating zone, and III holding zone in order to enable the charge heating rate to be controlled, and the required temperature to be obtained throughout the volume of the charge after heating. Heating blooms in furnaces at an excessively high heating rate may lead to stresses that can cause internal and external cracks, thereby hindering the downstream manufacturing process.

Heating should be carried out in as short time as possible, which restricts the grain growth, reduces decarburization, and limits a steel loss resulting from oxidation. In the furnace, wherein oxidation cannot be avoided, the furnace atmosphere impacts the heated material, which leads to scale formation and decarburization. The mass of the forming scale depends on the temperature and time of heating, furnace atmosphere, steel chemical composition, and gas velocity in the furnace chamber. Scale is a harmful effect as it causes steel loss, and during rolling, it can be pressed into the material surface, thereby lowering the quality of rolled products. In addition, scale reduces heat transfer, which causes a decrease in the heating rate and an increase in the heat consumption, or it leads to a decrease of temperatures in the charge cross-section [1] when maintaining a constant heating time. Determination of the optimal times of keeping the charge in individual heating zones of the furnace allows the scale thickness to be reduced, while heating the charge to the required temperature.

Based on the available literature describing the steel charge heating processes in industrial furnaces, we can distinguish a few methods applied for its optimization. The simplest models describing heat transfer in industrial furnaces use the zonal method [2-6]. These models apply constant wall temperatures and consider heat transfer by radiation between the furnace and the charge heated. More advanced models consider the flow of flue gas through the furnace chamber and heat transfer by convection [7]. Analyses of charge heating in a rotary hearth furnace using numerical packages, such as Matlab or CFD, can be found in the papers [8-11]. However, that models do not allow for thermal stress determination. It is important in the case of blooms obtained form the continuous casting process, which have a limited ductility. Moreover, that models do not consider the scale formation on the charge surface during heating. For that reasons have a limited applicability in the metallurgical industry.

In the paper the finite element method described in [13] was applied for modeling the charge heating process in a rotary hearth furnace.

2. Model of charge heating in a rotary furnace

Heat transfer in a rotary heart furnace with an outer diameter of 10.5 m, fired with natural gas, was analyzed. The furnace atmosphere temperature varied from 470°C to 1250°C. It is assumed that the furnace has a control system to enable the required flue gas temperature distribution to be maintained as well as the heating time to be controlled with the frequency of the furnace hearth shift time and the shift angle. The furnace bottom is made of ceramic materials and the walls and roof of the furnace are lined with refractory and insulation materials.

Charge heating was computed with a computer program using the finite element method [13] to solve a three-dimensional equation of heat conduction [14]:

$$\frac{\partial}{\partial x_1}\left(\lambda(t)\frac{\partial t}{\partial x_1}\right)+\frac{\partial}{\partial x_2}\left(\lambda(t)\frac{\partial t}{\partial x_2}\right)+ + \frac{\partial}{\partial x_3}\left(\lambda(t)\frac{\partial t}{\partial x_3}\right)+\dot{q}_v=\rho(t)c(t)\frac{\partial t}{\partial \tau} \quad (1)$$

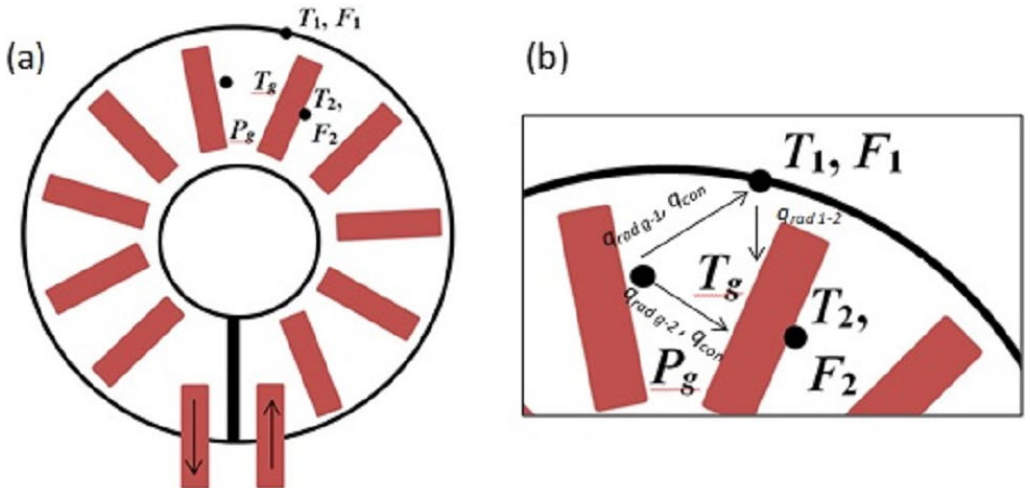

Fig. 1. (a) diagram of the rotary furnace chamber, (b) heat transfer model

In furnaces fired with natural gas, wall and gas body radiation is the prevailing mechanism of heat transfer. Convection arising from the flue gas movement has a smaller share in the thermal energy transfer. A simplified model was applied to describe the heat transfer within the furnace chamber, in which the furnace chamber, at a specific time τ, is considered a closed system consisting of two isothermal surfaces and an isothermal gas body at a specific time τ. Isothermal surfaces are the charge surface F_2 and the furnace wall surface F_1. However, the total chamber surface is divided by the number of blooms charged to the furnace. It has allowed to obtain the F_1 surface specific for a one bloom only. The model assumes that the density of the gas emissions reaching both surfaces is the same and the transparency of the gas body on the charge surface P_g is the same.

The heat flux absorbed by the charge surface (Figure 1b) was calculated from the equation:

$$\begin{aligned}&\dot{q}_2(\tau)=\dot{q}_{con}(\tau)+\dot{q}_{rad\,g-2}(\tau)+\dot{q}_{rad\,1-2}(\tau)=\\&=\alpha_{gw}\left(T_g-T_2\right)+\varepsilon_g\varepsilon_w 5.67\cdot10^{-8}\left(T_g^4-T_2^4\right)+\\&+\varepsilon_{sw}P_g 5.67\cdot10^{-8}\left(T_1^4-T_2^4\right)\end{aligned} \tag{2}$$

The emissivity of the steel charge surface ε_w was established from the formula [15]:

$$\varepsilon_w=1.2-0.52\frac{t_2}{1000} \tag{3}$$

The equivalent emissivity ε_{sw} of the walls-charge system was computed with the formula:

$$\varepsilon_{sw}=\frac{1}{\frac{1}{\varepsilon_2}+\varphi_{12}\left(\frac{1}{\varepsilon_1}-1\right)} \tag{4}$$

The average furnace wall temperature T_1 was calculated based on the flue gas temperature using the equation [16]:

$$\begin{aligned}&T_1=T_g-5.67\cdot10^{-8}\frac{1-\varphi_{12}}{\alpha_{g-1}}\\&\frac{\varepsilon_1\varepsilon_2}{\varepsilon_1+\varphi_{12}\varepsilon_2\left(1-\varepsilon_1\right)}\left[\left(T_1\right)^4-\left(T_2\right)^4\right]\end{aligned} \tag{5}$$

view factor φ_{12} was calculated using the equation [14]:

$$\varphi_{12}=\frac{F_2}{F_1} \tag{6}$$

The heat flux resulting from the flue gas body radiation was computed using the Hottel's model [17]. Under this theory, the transparency of a gas body with an absolute temperature T_g for radiation onto the charge surface was determined from the equation:

$$P_g=1-A_{g2} \tag{7}$$

where:

$$A_{g2}=\left(A_{CO_2}\right)_2+\left(A_{H_2O}\right)_2-\left(A_{CO_2}\right)_2\cdot\left(A_{H_2O}\right)_2 \tag{8}$$

$$\left(A_{CO_2}\right)_2=\varepsilon_{CO_2}\left(\frac{T_g}{T_2}\right)^{0.65} \tag{9}$$

$$\left(A_{H_2O}\right)_2=\varepsilon_{H_2O}\left(\frac{T_g}{T_2}\right)^{0.45} \tag{10}$$

The symbol ε_{CO_2}, ε_{H_2O} denotes the equivalent emissivity of carbon dioxide and steam. The equivalent emissivity of carbon dioxide and steam for $800 < t_g < 1400$°C was computed from the Kostowski's equations [18]:

$$\varepsilon_i=1-\exp\left[-k_i\left(p_i l\right)^{n_i}\right] \tag{11}$$

The average thickness l of the combustion gases layer has been calculated from:

$$l=1.8(HB/\left(H+B\right)) \tag{12}$$

where, H – furnace height, m, B – furnace width, m.

Coefficients k_i are described by equations:

- for steam partial pressure from p_{H_2O} 10 to 80 kPa

$$\begin{aligned}k_i&=0.03729-0.02375\left((T_g-273\right)/1000)\\n_i&=0.53\end{aligned} \tag{13}$$

- for carbon dioxide partial pressure: p_{CO_2} from 10 to 80 kPa

$$\begin{aligned}k_i&=0.07791-0.02573\left((T_g-273\right)/1000)\\n_i&=0.314\end{aligned} \tag{14}$$

Equivalent emissivity of flue gas ε_g was established from the formula:

$$\varepsilon_g=\varepsilon_{CO_2}+\beta\varepsilon_{H_2O} \tag{15}$$

$$\beta=1+\left(0.76-0.0328\sqrt{p_{H_2O}\cdot l}\right)\frac{p_{H_2O}}{100} \tag{16}$$

Heat flux resulting from the flue gas flow over the charge surface was determined from the Nusselt number:

$$q_{con}=\frac{Nu\lambda_s}{L}\left(T_g-T_2\right) \tag{17}$$

The value of the Nusselt number was determined from the relationship [14]:

$$Nu=0.037RePr_g^{0.43}\left(\frac{Pr_g}{Pr_s}\right)^{0.25} \tag{18}$$

The Reynolds number $Re=(w\cdot L)/v$ and the Prandtl number Pr_g were determined for the average temperature of the gas body T_g, the average flue gas velocity w and the average kinematic viscosity v. However, the value of the Prandtl number Pr_s was determined for the flue gas temperature equal to the charge surface temperature T_2.

The heat transfer coefficient at the furnace wall was calculated from the formula [14]:

$$\alpha_{g-1}=\frac{5.67\cdot10^{-8}\varepsilon_1\varepsilon_g}{T_g-T_1}\left[\left(T_g\right)^4-\left(T_1\right)^4\right] \tag{19}$$

Using the derived relationships, the effective heat transfer coefficient α_w was computed on the charge surface considering

the radiation of the walls, radiation of the flue gas body, and the flue gas movement around the charge:

$$\alpha_w = \frac{\dot{q}_2}{t_g - t_2} \tag{20}$$

The average temperature of the charge was computed from the formula:

$$t_2 = \frac{1}{L_w B_w} \int_0^{L_w} \int_0^{B_w} t(x_2, x_3) dx_2 dx_3 \tag{21}$$

The obtained heat transfer coefficient does not take account of the formation of an iron oxide layer on the charge surface. The calculations of the scale layer growth were conducted with oxidation kinetics equations developed based on the experimental research by R. Kuziak et al. [19]. In the boundary condition model for charge heating, equations allowing the oxidized layer thickness g_z (in millimeters) to be established as a function of heating time τ. This equation has the form [19]:

$$g_z = \frac{84.4}{\rho_z}\left[\exp\left(-\frac{9983}{T_2}\right)\right]\tau^{0.5} \tag{22}$$

where: $\rho_z = 5800$ kg/m^3 [20].

Based on the established scale layer thickness, at each computing step, the adjustment of the effective heat transfer coefficient is made α_w and the equivalent heat transfer coefficient α_2 occurring in the boundary condition of charge heating is calculated:

$$\alpha_2 = \frac{1}{\frac{1}{\alpha_w} + \frac{g_z}{\lambda_z}} \tag{23}$$

In the case of charge hated in the vertical position, adiabatic conditions have been assumed at the bottom surface of the charge. In the case of a round charge hated in the horizontal position at the charge surface facing the furnace hearth, radiation of the furnace walls as well as the gasses radiation have been neglected.

Validation of the boundary condition models has been given in [12]. A good agreement between the experimental data and numerical calculations was obtained during heating the charge in a rotary furnace. The temperature measurements of the charge heated in the industrial furnace have been conducted at selected points near the bottom as well as near the upper surface of the charge.

3. Model of stresses occurring during heating

In the charge heating process, the occurrence of stress is primarily related to the uneven charge temperature field and phase transformations in the solid state. Thermal stresses can be established after determining the temperature field. Thermal strains were computed with the finite element method using the methodology described in the paper [15]. The temperature field in the material heated over time changes and it is necessary to use the incremental method to determine stresses. The formation and development of cracks in the steel charge heated is a complex issue and it is difficult to define theoretically. However, there are approximate methods allowing the possibilities for crack occurrence to be assessed. For this purpose, the Ricea and Tracy criterion was applied:

$$\bar{\varphi}_f = C_{RT} \exp\left(-\frac{3}{2}\frac{\sigma_m}{\sigma_p}\right) \tag{24}$$

The paper [21] shows the suitability of this criterion for predicting the ductile crack formation in materials. The criterion anticipates the crack occurrence when the right-hand side of the criterion (24) has a value higher than the logarithmic strain $\bar{\varphi}_f$ established in the uniaxial tensile test. The constant C_{RT} is determined based on the stress and strain state in the uniaxial tensile test. As, during heating, the material can also deform when loaded with compressive strains, which does not lead to crack development, it is necessary to determine the limit strain in accordance with the formula:

$$\bar{\varphi}_f = \exp(0.5)\exp\left(-\frac{3}{2}\frac{\sigma_m}{\sigma_p}\right) \text{ for } \sigma_m > 0$$
$$\bar{\varphi}_f = 0 \text{ for } \sigma_m < 0 \tag{25}$$

To determine thermal stresses and strains, a method was applied, which has the following primary stages [15]:

- Determination of the displacement field as a function of element node displacements caused by the uneven temperature field and phase transformations in accordance with the course of the thermal expansion coefficient.
- The transfer of displacements from the nodes to the area of an element is obtained with linear shape functions.
- The displacement field is determined as a function of derivative node displacements.
- Stresses arising from the node displacements are determined based on the Prandtl-Reuss elastic-plastic deformation theory.

4. Numerical computing

Changes in the temperature of the material that was heated were computed for charges with dimensions featuring a considerable length in relation to the diameter. Three steels with different chemical compositions were tested, as shown in Table 1. Stainless steel 1.4307 belongs to the group of steels resistant to oxidation. Based on the data from the paper [22], the models of thermal conductivity, specific heat, and density as functions of temperature were developed. Steel properties are shown in Figure 2-4.

The numerical calculations of the heating process were performed assuming 4 heating curves, differing with the temperature range within individual heating zones (Fig. 5). The heating curves

TABLE 1

Chemical composition of steels – percentage share of alloying elements

	Element percentage share, %									
Steel	**C**	**Mn**	**Si**	**P**	**S**	**Cr**	**Ni**	**Mo**	**Cu**	**Al**
1.7225	0.38-0.45	0.60-0.90	max 0.40	max 0.025	max 0.035	0.90-1.20	—	0.15-0.30	—	—
1.7380	0.08-0.15	0.40-0.60	0.15-0.40	max 0.030	max 0.030	2.00-2.50	max 0.30	max 0.30	max 0.25	max 0.02
1.4307	max 0.07	max 2.00	max 1.0	max 0.045	max 0.03	17.5-19.5	8.0-10.5	—	—	-

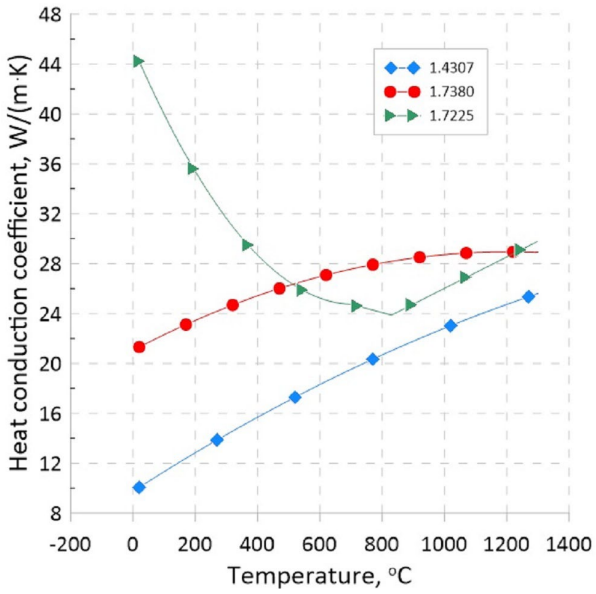

Fig. 2. Heat conduction coefficient as function of temperature for of the steels analyzed

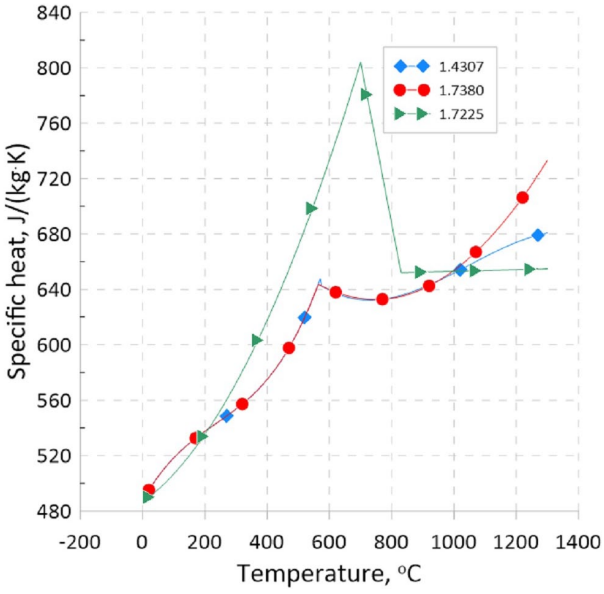

Fig. 3. Specific heat as function of temperature for of the steels analyzed

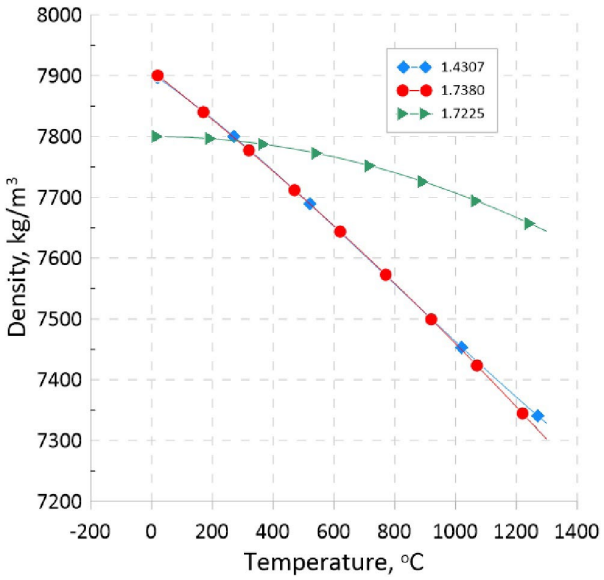

Fig. 4. Density as function of temperature for of the steels analyzed

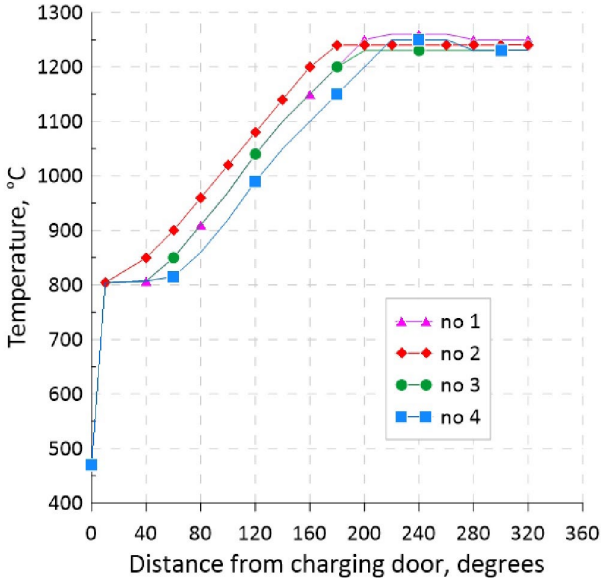

Fig. 5. The furnace temperature variation

have been proposed using a trial-and-error method as well as the knowledge resulting from the cooperation with the industry. The initial round bloom temperature was assumed of 20°C. Heating was performed until the temperature of 1200°C was obtained at the charge axis. The number of the furnace hearth shifts was 65. It is limited by the number of ingots charged into the furnace. However, the shift time has been determined due to numerical simulations of the charge temperature. The selected heating curves allowed the impact of temperature and time of staying in each heating zone on the scale growth, heating rate, and thermal stress to be analyzed. The analysis has resulted in selecting the heating process with the highest efficiency. The division of

the furnace chamber into zones with appropriate lengths and the correct flue gas temperature distribution in the furnace, compliant with the specificity of heating furnace operation, contributes to reducing the energy consumption of the heating process. However, it may be advantageous only for a single group of steels. Therefore, for furnaces executing the heating process with a large variability of steel grades, it is important to know the possibilities of managing the furnace to enable furnace operating parameters to be changed, advantageously for individual types of materials.

Numerical computing for the charge of steel 1.7225 was made for the horizontal and vertical charge arrangements. The other analyses were made for the charge placed laying on the furnace bottom. The dimensions of the charge tested were Ø813 × 2189 mm. The results of numerical computing were presented in the form of temperature change in 6 selected points, as shown in Figure 5, and in the form of a temperature field on the longitudinal section. In addition, a change in the thermal power absorbed by the charge from the flue gas and furnace walls, the thickness of the oxidized layer, change in the heat transfer coefficient during the process, and the charge temperature growth rate were determined.

The charge arrangement influences the amount of the heat transferred and the heating time. Results of calculations for the charge of steel 1.7225, heated according to curve no. 1, and placed in the horizontal and vertical position are shown in Figures 6-12. The heat transfer coefficient changes as the heating zone changes. In the preheating zone, it achieves low values due to the weak radiation of the gas body and furnace

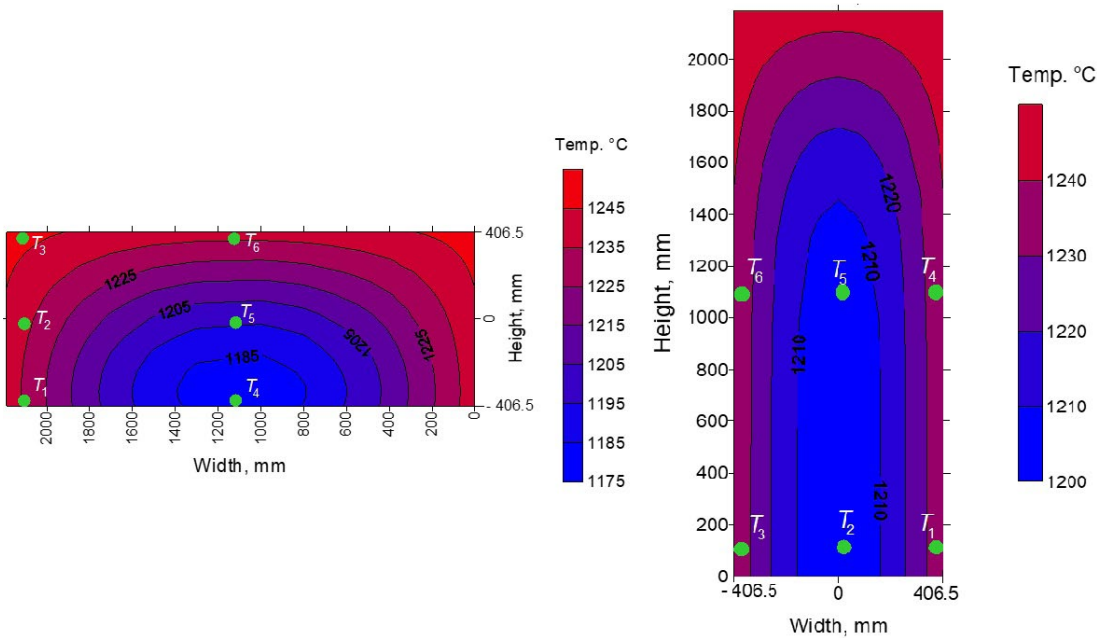

Fig. 6. The temperature field in the cross-section of the steel 1.7225 at the end of process for the furnace temperature variation no. 1

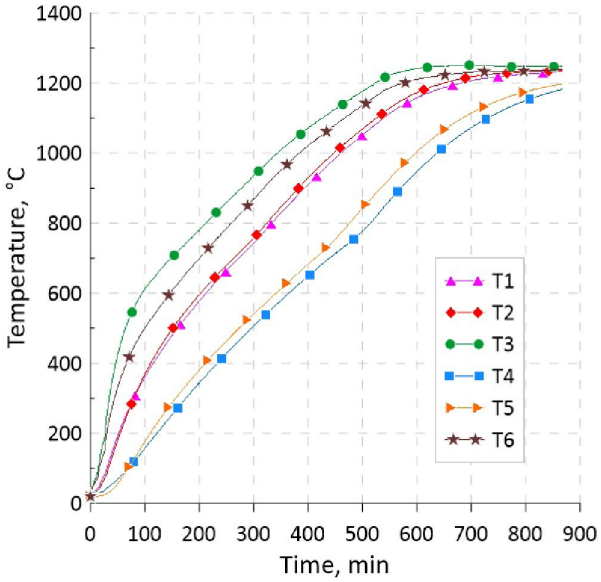

Fig. 7. Temperature change of the charge of steel 1.7225, heated according to curve no. 1, placed in the horizontal position

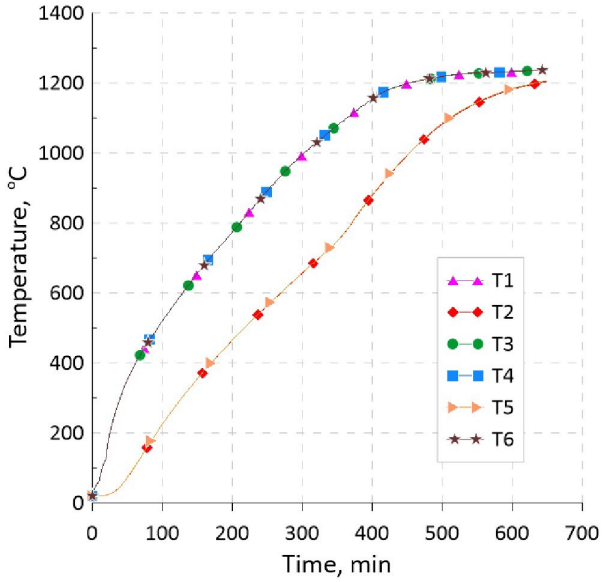

Fig. 8. Temperature change of the charge of steel 1.7225, heated according to curve no. 1, placed in the vertical position

walls, and in the heating zone, it reaches the maximum value of 425 W/(m^2 K). In the holding zone, the heat transfer declines due to an increase in the scale thickness and a high temperature of the charge surface. For the vertical charge, heating is uniform on the charge circumference. For the horizontal charge, the slowest temperature increase is at the half of the length of the charge, at a contact place of the charge with the bottom, and on the axis. The fastest increase is observed at the surface from the roof side (Fig. 7). In the case of a charge placed in the vertical position, the lowest temperatures are observed on the axis (Figs 6, 8). The heating time in the vertical position until the required temperature has been obtained is approx. 3.5 h shorter than for the horizontal charge (Table 2). In both cases, the fastest scale growth is observed after exceeding the temperature of approx. 700°C (Fig. 10). For steel heating, parameters determining the steel loss for scale include time, temperature, and the furnace chamber atmosphere [23,24]. The obtained thickness of scale is in a good agreement with the experimental data [24]. The maximum heating rates are achieved in the heating and preheating zones, and they are not exceeding 4 K/min. for the charge in the horizontal position (Fig. 11) and 40 K/min. for the vertical charge. Heating of blooms in the vertical position requires an adequately high furnace, fitted with dedicated loading and unloading facilities and the mounting ensuring a stable position during hearth rotation. The charge heating in the vertical position is recommended only for a short blooms. In other cases, a system stabilizing the charge in the furnace is required [25]. In such a case only a small part of the charge surface is under the adiabatic boundary conditions. Charge heated in the horizontal position, laying on the furnace

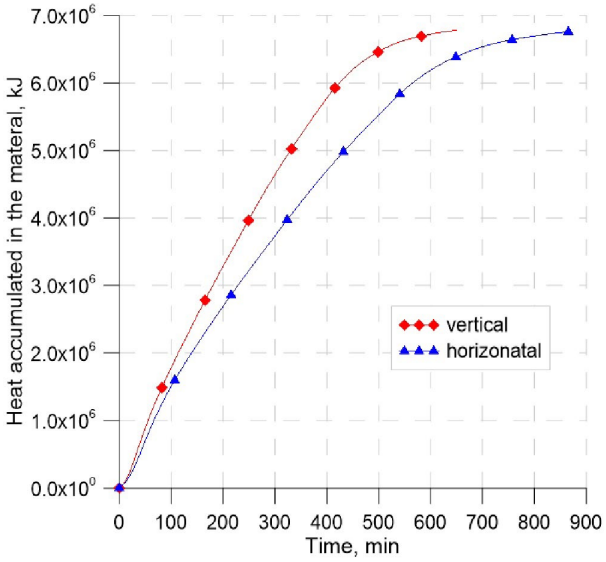

Fig. 9. Change in energy absorbed by the charge of steel 1.7225 placed in the horizontal and the vertical positions

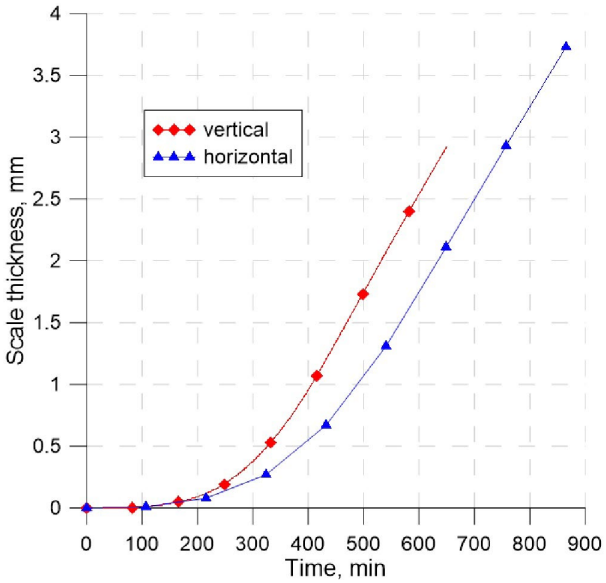

Fig. 10. Comparison of scale thickness growth during the heating process of charge of steel 1.7225 placed in the horizontal and vertical positions

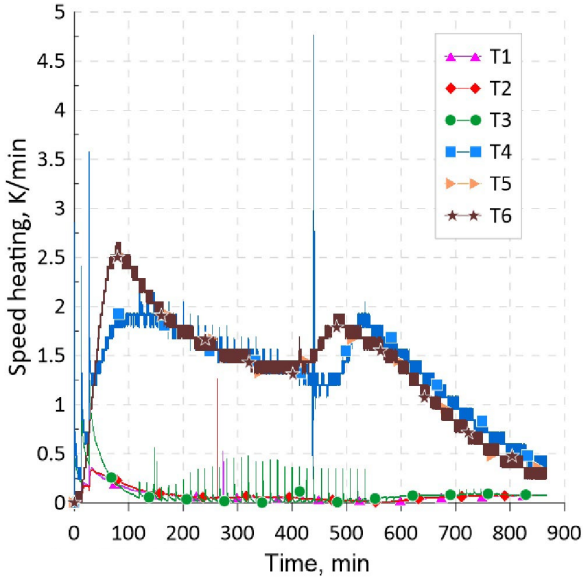

Fig. 11. Heating rate of the charge of steel 1.7225 placed in the horizontal position

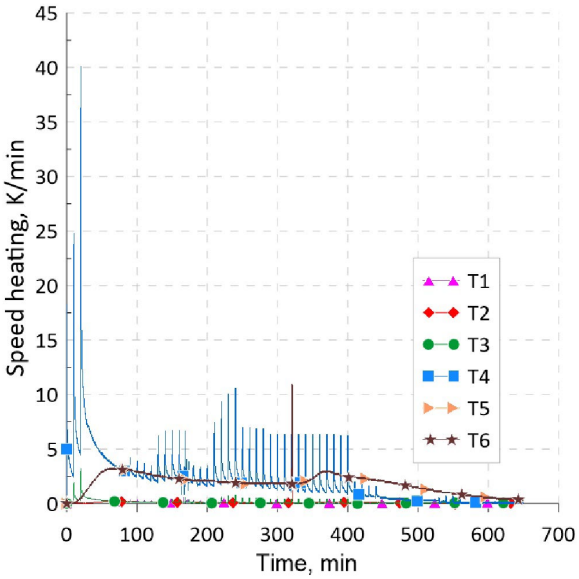

Fig. 12. Heating rate of the charge of steel 1.7225 placed in the vertical position

bottom, has considerably lower heat transfer at a larger part of the surface facing the furnace hearth.

Results for the other analyzed variants for the horizontal position are summarized in Table 2. The results refer to the values obtained at the end of the process. The recommended strategy of the charge heating has been obtained as a result of a several simulations. A trial-and-error method has been employed to meet the desired temperature at the charge axis. The shortest heating time for the steels analyzed was obtained for the charges heated according to heating curve no. 1. The lowest scale thickness was also obtained for this curve. In the case of change of the furnace temperature according to curve no. 2, an insignificantly longer heating time was obtained for steel 1.7380, but the scale thickness at the process end increased by 0.3 mm. The temperature increase in the heating and preheating zones by 50°C did not affect the heating rate for steel 1.7225. For both mentioned steels, the shift time was 800 s. A low heating rate in this case was due to the scale thickness increase resulted from the high furnace temperature. As a result of that the insulation effect of the scale was essential.

A round bloom of steel 1.4307 required extending the heating time by 1 h, and the shift time was 900 s. It was due to a low conductivity of this grade of steel and a higher specific heat of 1.7225 steel, (Figs 2-4). Heating the charge according to curve no. 3 and 4 extended the time of heating by approx. 2-3 h. The proposed heating curves has resulted form the knowledge gained from the cooperation with the steel industry and numerical simulations. Only the heating curves applicable in the rotary hearth furnace have been analyzed.

The thermo-physical properties of a material influence the rate of heat transferred and the material thermal capacity of the system. For the steels tested, steel 1.7225 was the one

TABLE 2

Heating parameters

Steel grade	The furnace temperature variation	Heating time, min.	Minimum temp. °C	Maximum temp. °C	Scale thickness, mm	Indexing time, s
1.7225 horizon	no. 1	866	1181	1248	3.7	800
	no. 2	866	1180	1238	3.9	800
	no. 3	1029	1190	1228	4.2	950
	no. 4	1029	1187	1229	4.0	950
1.7225 vertical	no. 1	650	1204	1248	2.9	600
1.7380	no. 1	845	1189	1248	3.7	780
	no. 2	866	1192	1238	4.0	800
	no. 3	975	1191	1228	4.1	900
	no. 4	975	1188	1229	3.8	900
1.4307	no. 1	920	1178	1248	—	850
	no. 2	975	1189	1238	—	900
	no. 3	1083	1188	1229	—	1000
	no. 4	1083	1184	1229	—	1000

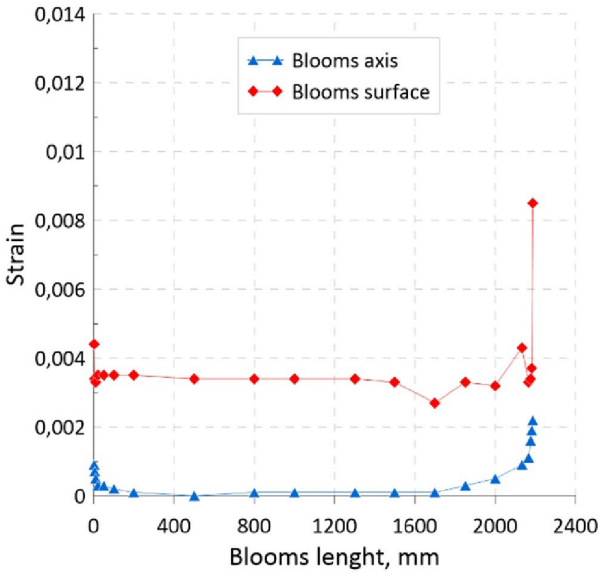

Fig. 13. Effective strain at the axes and surface for the charge of steel 1.7225 placed in the horizontal position at the half time of the heating process

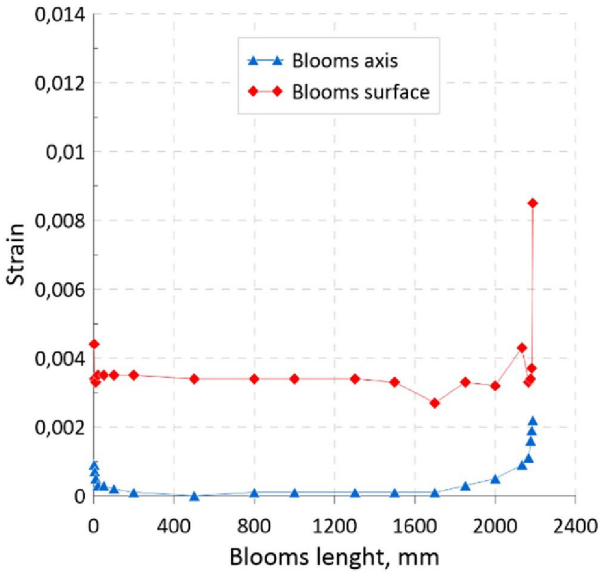

Fig. 14. Effective strain for at the axes and surface for the charge of steel 1.7225 placed in the vertical position at the half time of the heating process

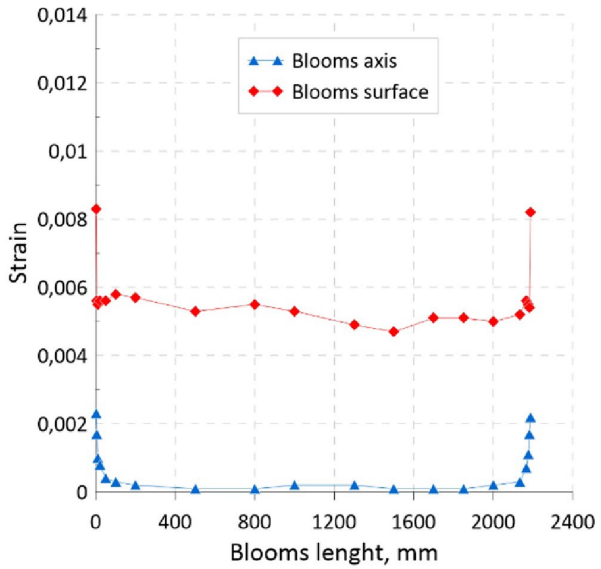

Fig. 15. Effective strain at the axes and surface of the charge of steel 1.7225 placed in the horizontal position at the end of the heating process

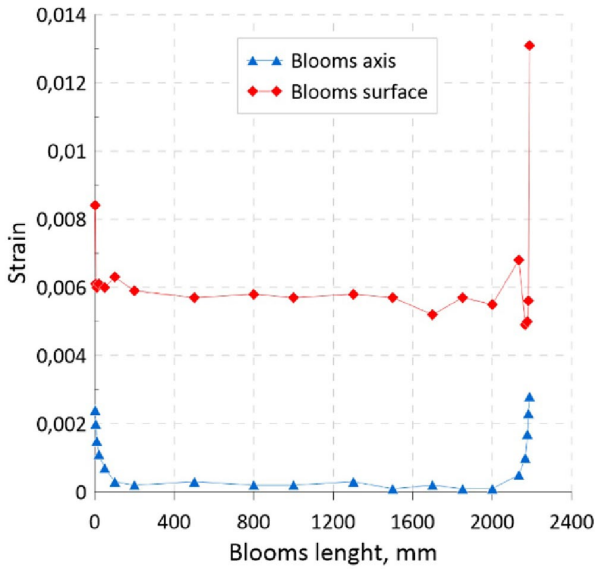

Fig. 16. Effective strain at the axes and surface of the charge of steel 1.7225 placed in the vertical position at the end of the heating process

that absorbed heat most intensively (Fig. 11), and steel 1.4307 was the one that absorbed heat at the slowest rate. To obtain the same temperature, a bloom of steel 1.7225 required by $45 \cdot 10^7$ kJ more heat to be supplied than a bloom of steel 1.4307. The rate of energy absorbed by the charge also depended on the assumed heating curve. These differences caused an increase in the heating time between the charge tested by approx. 1 h for heating curve no. 1 to approx. 2 h for curve nos. 3 and 4.

Numerical computing of the stress field was conducted for the charge made of steel 1.7225 in the horizontal arrangement and for the vertically arranged charge for heating curve no. 1 shown in Fig. 5. The thermal stress model required the following parameters to be established: Young modulus E, Poisson ratio ν, linear expansion coefficient β, and yield stress σ_p as a function of temperature.

The completed calculations and their analysis have showed a maximum value of the parameter $\overline{\varphi}_f$ of 0.014 (Figs 13-16). Distributions of strain intensities allow us to find that dangerous tensile stresses do not occur in the heating process. However, it is necessary to compare the computed maximum strain to the one determined by a cold tensile test. The critical value of the $\overline{\varphi}_f$ factor for a steel charge varies from 0.05 to 0.1. Thus, the probability of the charge fracture is low for the proposed heating strategy.

5. Conclusions

The numerical computations have been performed to optimize the charge heating process. A trial-and-error method has been employed to optimize the charge heating in the rotary furnace. The heat transfer boundary conditions employed in the numerical model has been validated based on the charge temperature measurements in the industrial furnace.

The proposed heating curves have resulted from the knowledge gained during the cooperation with the steel industry. Only heating curves possible for the implementation in the rotary furnace have been analyzed.

The numerical computations of the charge temperature and the scale thickness have allowed to determine the lowest heating time for a particular grade of steel and the charge dimensions. Moreover, it has been shown that the possibility of the charge fracture is low.

It has been shown that the charge heating in the vertical position is the best choice. However, it is limited by the charge shape and dimensions.

Acknowledgements

Financial assistance of NCBiR within the project INNOSTAL, agreement no. POIR.01.02.00-00-0086/19 is acknowledged.

REFERENCES

[1] M. Kieloch, J. Boryca, B. Halusiak, Hutnik, Wiadomości Hutnicze **78** (5), 446-448 (2011).

[2] R. Gruszka, Z. Rudnicki, Archiwum Hutnictwa **21** (4), 613-631 (1976).

[3] H. Ebrahimi, A. Zamaniyan, J.S.S Mohammadzadeh, A.A Khalili, Applied Mathematical Modelling **37** (16-17), 8004-8015 (2013).

[4] A. Emadi, A. Saboonchi, M. Taheri, S. Hassonpur, Applied Thermal Engineering **62**, 396-405 (2014).

[5] Y. Hu, C.K. Tan, J. Broughton, P.A. Roach, Applied Thermal Engineering **173**, 555-566 (2016).

[6] E. Blanco, J.M. Vargas, F. Medina, J. Paiuk, IFAC Proceedings Volumes **22** (11), 161-166 (1989).

[7] B. Mayr, R. Prieler, M. Demuth, L. Moderer, C. Hochenauer, Energy Procedia **120**, 462-468 (2017).
[8] V. Muresan, M. Abrudean, T. Colos, Modeling and Simulation of the billets heating process in a furnace with rotary hearth. In: 15th international conference on system theory, control and computing (2011).
[9] V. Muresan, M. Abrudean, IFAC Proceedings Volumes **45** (21), 735-740 (2012).
[10] M. Landfahrera, C. Schlucknera, R. Prielera, H. Gerhardtera, T. Zmekb, J. Klarnerb, C. Hochenauera, Energy **180**, 79-89 (2019).
[11] A. DellaRocca, M. Fantuzzi, V. Battaglia, E. Malfa, Steel Times International **9**, 1-5 (2012).
[12] A. Gołdasz, Z. Malinowski, T. Telejko, M. Rywotycki, A. Szajding, Archives of Metallurgy and Materials **57** (4), 1144-1149 (2012).
[13] Z. Malinowski, M. Głowacki, M. Pietrzyk, Archives of Metallurgy **39**, 277-294 (1994).
[14] A.Ç. Yunus, Heat and mass transfer, McGrawHill, New York (2007).
[15] Z. Malinowski, Numeryczne modele w przeróbce plastycznej i wymianie ciepła, Kraków, Wydawnictwa AGH (2005).
[16] T. Senkara, Wärmetechnische Rechnungen für gas-und ölbeheizte Wärmeöfen, Vulkan-Verlag (1977).
[17] H.C. Hottel Radiant Heat Transmission, in ed. W.H. McAdams Heat Transmission, McGraw-Hill, New York (1954).
[18] E. Kostowski, Gaswärme International **40**, 529-534 (1991).
[19] R. Kuziak, M. Głowacki, M. Pietrzyk, Z. Malinowski, XIV Konferencja Naukowo-techniczna Huty Katowice „Produkcja i Eksploatacja Szyn Kolejowych", Rogoźnik, 161-171 (1994).
[20] M. Li, R. Endo, M. Akoshima, M. Susa, Temperature Dependence of Thermal Diffusivity and Conductivity of FeO Scale Produced on Iron by Thermal Oxidation, ISIJ International **57**, 2097-2106 (2017).
[21] W.M. Garrison, N.R. Moody, Journal of Physics and Chemistry of Solids **48**, 1035-1074 (1987).
[22] N. Ju Tajc, Technologija nagreva stali. Metallurgizdat, Moskva (1962).
[23] M. Kieloch, The Effect of Heating Parameters on the Mass Loss of Steel. Archives of Metallurgy **41**, 35-50 (1996).
[24] I.W. Medvedeva, K.M. Pachalujev, O.I. Morgal, Kineticheskije charakterystiki vysokotemperaturnogo okislenija uglerodistych stalej, Stal **6**, 572 (1973).
[25] https://steel.fivesgroup.com/reheating/stein-helyo-rth-rotary-hearth-furnaces.html dostęp 6.03.2021.